Revista Mexicana de Astronomía y Astrofísica, **32**, 161–174 (1996)

A COMPILATION OF OPTICAL SPECTROPHOTOMETRY OF HH OBJECTS AND ITS TENTATIVE INTERPRETATION

A.C. Raga[1], K.-H. Böhm[2], and J. Cantó[1]

Received 1996 May 3; accepted 1996 August 6

RESUMEN

Este artículo presenta una compilación que incluye una parte considerable de todas las observaciones espectrofotométricas de objetos Herbig-Haro (HH) que han sido publicadas (por un número de distintos autores) desde 1981 a 1993. Nuestra compilación incluye 45 condensaciones de 31 distintos flujos, para las que han sido obtenidos espectros tanto azules como rojos (en el rango de $\sim$ 3700 Å a $\sim$ 8000-10000 Å). De este conjunto de datos, hemos elegido un número de cocientes de líneas ([O III] 5007/Hβ, [Ne III] 3868/Hβ, [O II] (3726+3729)/Hβ, [N II] 6583/Hβ, [O I] 6300/Hα, [N I] (5198+5200)/Hβ, [Ca II] 7291/Hα, [S II] (4068+4076)/Hβ y [S II] (6717+6731)/Hα) que no están afectados fuertemente por el enrojecimiento. Estudiamos las distintas correlaciones que se observan entre estos cocientes de línea y comparamos los resultados con predicciones de modelos de onda de choque.

También usamos nuestra compilación de espectros para derivar un criterio cuantitativo (basado en los cocientes [O III] 5007/Hβ y [S II] (6717+6731)/Hα) para dividir los espectros HH en categorías de alta, intermedia y baja excitación. Finalmente, obtenemos determinaciones empíricas de n_e (del cociente [S II] 6731/6717) para todas las condensaciones HH de nuestra muestra.

ABSTRACT

This paper presents a compilation that includes a large fraction of the spectrophotometric observations of Herbig-Haro (HH) objects published (by a number of different authors) from 1981 through 1993. Our compilation includes 45 separate condensations of 31 different outflows, for all of which both blue and red spectra (in the range from $\sim$ 3700 Å to $\sim$ 8000-10000 Å) are available. From this data set, we have chosen a number of line ratios (namely, [O III] 5007/Hβ, [Ne III] 3868/Hβ, [O II] (3726+3729)/Hβ, [N II] 6583/Hβ, [O I] 6300/Hα, [N I] (5198+5200)/Hβ, [Ca II] 7291/Hα, [S II] (4068+4076)/Hβ and [S II] (6717+6731)/Hα) which are not strongly affected by reddening. We then study the different correlations that are found between these line ratios, and compare the results with predictions from shock wave models.

We also use the compiled data set to derive a quantitative criterion (based on the [O III] 5007/Hβ and [S II] (6717+6731)/Hα line ratios) to divide HH spectra into the high, intermediate and low excitation categories. Finally, we obtain empirical determinations of n_e (from the [S II] 6731/6717 ratio) for the HH condensations of our sample.

Key words: **ISM–JETS AND OUTFLOWS — STARS–FORMATION**

[1] Instituto de Astronomía, Universidad Nacional Autónoma de México.
[2] Astronomy Department, University of Washington, USA.

1. INTRODUCTION

In recent years there has been considerable progress in our understanding of outflows from young stellar objects, their optical jets and their Herbig-Haro (HH) objects (see, e.g., the reviews by Edwards, Ray, & Mundt 1993, Reipurth & Heathcote 1993, Ray & Mundt 1993, Reipurth & Cernicharo 1995, and the survey of theoretical models by Raga 1995). In the recent past the main interest has been concentrated on the (probably) magnetohydrodynamic generation of the outflow, its place of origin, and on the interpretation of the geometry of outflows and jets. The explanation of the details of the optical (and uv) spectra of HH objects and jets has not played such an important role any more. The reason is obvious. There is a general belief that we understand the generation of HH spectra as caused by shock waves (Schwartz 1975) which are generated by the jet (bow shocks, jet shocks etc.) and that the generation of spectra in these shocks is (at least in a fundamental way) understood. This is true in general.

However, in a preliminary investigation of the spectra of HH objects for which the most detailed spectra are presently available (HH 1, HH 2H, HH 2A, HH 3, HH 24A, HH 32A, HH 255, HH 43B,C, HH 47A, HH 7, HH 11), Böhm (1995) came to a tentative but surprising conclusion. He found that among these objects all the high excitation objects show an [O III] 5007/Hβ ratio which is predicted for (plane) shock waves with a shock velocity smaller than ~ 95 km s^{-1}. In this (admittedly small) sample there is no indication (from the [O III]/Hβ ratio) of any larger shock velocity. If we make the comparison with bow shock models (Hartigan, Raymond, & Hartmann 1987) the limit corresponds to about 120 km s^{-1}. This conclusion would seem to be quite surprising especially since it seems to be confirmed by the [Ne III]/Hβ ratio and probably by the [S III]/Hα ratio. The next question is of course: Does this apply to all HH objects? It therefore seems to be well justified to look at a larger sample of spectra of HH objects and also to try to draw some more general conclusions about these spectra and the (possibly) unexpected aspects of their shock wave interpretation.

In order to do this we used the presently available literature about spectrophotometric data of HH objects (as described below). The drawback of this approach is that we have to combine spectrophotometric observations of different (spectral) resolution and different signal to noise ratios. Consequently we have to restrict our investigation to relatively few strong and moderately strong lines which (in principle) could be detected in all spectra available to us. This excludes a number of interesting problems (which must be clarified in later studies) like e.g., the enigmatic behaviour of the [C I] (9823,9849) lines in low excitation HH objects. In the following sections we shall show that even our present, relative modest approach leads to a number of unexpected statements about the properties of Herbig-Haro shock waves.

2. THE DATA SET

We have used the catalogue of Reipurth (1994), which gives a comprehensive list of references for the numbered HH objects, to compile a list of all of the papers on spectroscopical observations of these objects. From these papers, we have chosen the HH objects for which both red and blue spectra have been obtained, and for which at least ~ 10 line fluxes are given. In the cases in which a number of papers give the spectrum of the same object, we have taken the results from the most recent reference.

In some cases, spectra are available for different condensations of the same outflow (e.g., HH 7, 10 and 11; HH 2A, G and H; HH 43A, B and C). As the different condensations of the same outflow many times have spectra with very different excitations, we have included all of the spectra of the individual condensations in our tabulation. In this way, we have obtained a tabulation of a chosen set of emission lines for 45 condensations of 31 different outflows (counting the red- and blue-shifted lobes from the same source as separate outflows).

Table 1 gives the fluxes of the blue spectrum emission lines [O II] (3726+3729), [Ne III] 3868, [S II] (4068+4076), [Fe III] 4658, [O III] 5007, [Fe II] 5158, [N I] (5198+5200), and [Fe II] (5262+5273) and the red spectrum emission lines [O I] 6300, Hα, [N II] 6583, [S II] 6717, [S II] 6731, [Fe II] 7155, [Ca II] 7291, the [O II] 7319+[Ca II] 7324+[O II] 7330 blend, [S III] 9069, [S III] 9532 and [C I] 9849. These lines have been chosen in order to cover a range of excitations, and to illustrate different effects found in the spectra of HH objects. Table 1 also gives the references from which the spectra have been obtained.

Clearly, many of these lines have not been detected in all of the HH objects of our sample. In the cases in which the UV and/or the IR part of the spectrum has not been observed, we have indicated the absence of line detections with a "—" in the corresponding place (see Table 1). In other cases, we find that some papers do not appear to have a complete tabulation of the detected lines (restricting themselves to a few "interesting" lines), so that we have also indicated the missing lines with a "—". Other papers do appear to have a complete list of all of the detected lines, and in these cases we have indicated the absence of detected emission by giving the line flux a value of zero.

Finally, for many objects we have listed two values of the emission line fluxes (in both cases, with respect to Hβ = 100), the first set (in the same line of text as the identification of the object, see Table 1) cor-

TABLE 1

BLUE AND RED SPECTRA OF HH OBJECTS RELATIVE TO Hβ = 100

HH	[O II] 3726/8	[Ne III] 3868	[S II] 4068/76	[Fe III] 4658	[O III] 5007	[Fe II] 5158	[N I] 5198/200	[Fe II] 5262/73	[O I] 6300	Hα 6563	[N II] 6583	[S II] 6716	[S II] 6731	[Fe II] 7155	[Ca II] 7291	[O II]+[Ca II] 7325	[S III] 9069	[S III] 9532	[C I] 9849
1	139	11	63	3	60	25	18	19	248	508	247	108	177	56	83	135	6	14	18
	211	15	83	4	57	22	16	15	159	311	151	64	105	31	45	67	3	6	7
2A	149	10	49	8	118	4	12	9	164	520	233	102	...	36	...	146	...	20	36
	211	14	61	9	109	4	11	8	110	335	115	64	...	22	...	84	...	10	16
2G	113	9	66	5	39	6	26	21	239	466	195	142	...	55	...	98	...	...	26
	170	13	87	5	35	5	22	17	149	278	116	83	...	30	...	51	...	...	10
2H	122	10	52	6	68	...	11	12	176	438	231	58	103	35	...	111	...	16	17
	169	13	64	7	63	...	10	10	122	293	154	38	67	22	...	67	...	8	8
3	126	...	17	...	48	...	17	...	108	485	157	111	219	...	33	40	...	...	23
	194	...	22	...	44	...	15	...	67	285	92	63	125	...	17	21	...	...	9
7[a]	89	...	171	0	0	24	286	9	577	435	34	868	745	10	86	56	0	0	1059
10	...	...	79	0	0	32	200	0	744	661	144	777	772	58	222	...	...	...	...
11[a]	141	...	79	0	0	29	101	30	241	307	52	211	261	30	88	62	0	0	87
24A	71	...	39	...	26	19	36	16	221	528	168	179	246	14	12	...	...	...	...
	139	...	60	...	22	15	28	12	103	228	72	74	101	4	4	...	...	...	...
30	...	...	...	...	0	...	30	...	526	813	132	358	443	...	...	...	...	...	...
32	206	9	48	8	94	16	16	21	214	557	411	201	326	35	49	119	26	53	65
	396	16	73	9	85	13	13	16	102	247	181	85	137	14	18	43	9	12	15
34(ap.)	306	12	13	0	54	7	17	5	85	435	58	120	83	5	29	36	...	...	...
	474	18	18	0	52	6	15	4	60	292	39	78	54	3	17	21	...	...	...
34(MD)	185	0	21	0	14	19	56	8	190	478	68	269	186	13	86	53	...	...	...
	286	0	29	0	13	17	50	7	133	320	45	175	121	8	50	31	...	...	...
34(jet)	0	0	102	0	0	160	379	78	1763	610	72	2055	1798	260	628	406	...	...	...
	0	0	141	0	0	145	339	69	1235	409	48	1335	1165	156	368	236	...	...	...
40	138	6	26	...	69	29	30	16	161	512	208	389	...	...	39	...	...	...	...
	267	10	41	...	60	26	24	12	76	214	91	163	...	...	14	...	...	...	...
43A[a]	253	0	36	0	48	4	21	3	97	341	86	77	81	3	6	15	0	0	20
43B[a]	0	0	38	0	0	8	111	3	287	480	95	336	320	5	16	16	0	0	228
43C[a]	0	0	44	0	0	3	135	0	476	526	66	391	376	4	23	13	0	0	270
47A	81	0	77	...	0	...	129	...	342	500	72	486	511	...	125	71	...	...	...
	87	0	81	...	0	...	127	...	320	463	67	448	471	...	113	64	...	...	...
47C	30	0	35	...	0	...	83	...	236	670	98	350	270	...	0	0	...	...	...
	48	0	48	...	0	...	73	...	150	390	57	197	152	...	0	0	...	...	...
47D	1420	0	0	...	190	...	107	...	344	690	430	990	420	...	161	117	...	...	...
	1630	0	0	...	187	...	103	...	302	590	369	840	360	...	132	96	...	...	...
49	192	...	16	...	66	9	0	0	43	373	82	35	42	0	0	36	...	...	...
	283	...	21	...	64	8	0	0	30	243	54	22	27	0	0	21	...	...	...
50	98	...	7	...	10	0	0	0	81	526	122	131	127	0	0	89	...	...	...
	198	...	11	...	9	0	0	0	41	242	56	57	55	0	0	32	...	...	...
54B	138	...	18	...	9	29	57	16	460	727	350	366	371	51	133	146	...	...	...
	332	...	31	...	8	24	46	12	211	299	143	142	143	17	43	46	...	...	...
54C	174	...	22	...	42	36	105	0	587	972	398	616	558	89	213	197	...	...	...
	505	...	45	...	37	28	80	0	210	302	122	177	159	21	47	43	...	...	...

1996RMxAA..32..161R

TABLE 1 (CONTINUED)

HH	[O II] 3726/8	[Ne III] 3868	[S II] 4068/76	[Fe III] 4658	[O III] 5007	[Fe II] 5158	[N I] 5198/200	[Fe II] 5262/73	[O I] 6300	Hα 6563	[N II] 6583	[S II] 6716	[S II] 6731	[Fe II] 7155	[Ca II] 7291	[O II]+[Ca II] 7325	[S III] 9069	[S III] 9532	[C I] 9849
56	180	...	45	...	49	20	54	11	356	552	210	259	315	24	45	51	...	...	...
	328	...	67	...	46	18	46	9	199	286	108	128	156	11	19	22	...	...	...
57	185	...	...	...	0	0	61	0	328	744	225	328	356	0	0	...	...	...	...
	433	...	...	...	0	0	49	0	143	290	87	120	130	0	0	...	...	...	...
83B,D	282	7	29	...	11	13	34	13	185	476	170	253	242	66	56	...	...	...	...
	422	11	39	...	11	12	30	11	119	288	103	148	141	35	29	...	...	...	...
111V	42	0	15	0	0	4	59	0	181	594	58	311	271	0	6	17	...	...	...
	89	0	26	0	0	3	49	0	99	298	29	149	129	0	2	7	...	...	...
111L	43	0	25	0	12	22	81	22	298	723	80	419	350	33	93	74	...	...	...
	112	0	51	0	10	18	63	16	136	298	33	163	135	11	29	23	...	...	...
111D-J	21	0	104	0	0	65	268	27	1180	987	206	1495	1508	166	349	263	...	...	...
	55	0	211	0	0	52	209	19	540	407	84	580	582	54	108	80	...	...	...
123	60	...	111	...	19	...	24	...	440	915	100	88	143	35	14	115	...	...	...
	90	...	140	...	18	...	21	...	300	590	67	55	90	20	8	65	...	...	...
124A-C	259	...	25	...	19	...	32	...	128	535	164	255	231	...	...	...	...	...	...
	436	...	36	...	18	...	28	...	76	293	89	134	121	...	...	...	...	...	...
124D	213	...	27	...	46	...	17	...	...	342	117	116	79	...	...	...	...	...	...
	242	...	29	...	46	...	16	...	...	292	100	98	67	...	...	...	...	...	...
124E-F	386	...	23	...	0	...	17	...	...	290	173	182	159	...	...	...	...	...	...
	393	...	24	...	0	...	17	...	...	284	170	178	155	...	...	...	...	...	...
125F	466	...	...	...	0	...	39	...	166	413	215	342	203	...	...	...	...	...	...
	614	...	...	...	0	...	35	...	122	293	152	237	140	...	...	...	...	...	...
125I-K	206	...	...	...	0	...	97	...	308	503	119	423	342	...	...	...	...	...	...
	318	...	...	...	0	...	84	...	191	292	69	236	191	...	...	...	...	...	...
126B	222	...	...	...	17	...	...	...	27	387	72	74	60	...	...	...	...	...	...
	280	...	...	...	16	...	...	...	21	290	54	54	44	...	...	...	...	...	...
128	177	...	85	...	0	...	324	...	651	649	76	1382	1118	...	...	...	...	...	...
	353	...	141	...	0	...	259	...	306	275	32	552	444	...	...	...	...	...	...
154	...	...	...	...	98	0	35	...	1477	2500	1310	803	1578	546	1507	1387	...	...	...
158	...	...	...	...	28	39	13	...	114	378	188	92	169	...	...	...	...	...	...
184	...	...	...	...	17	0	0	0	369	2074	259	115	215	0	0	0	...	...	...
234	...	...	...	...	42	0	38	0	189	574	146	284	230	65	166		...	...	...
235	...	...	...	...	0	18	38	12	258	582	197	333	255	37	164		...	...	...
240	...	...	...	...	33	34	39	23	374	578	230	274	336	89	313		...	...	...

[a] Only the dereddened fluxes are listed.

1: Solf, Böhm, & Raga (1988).
2, 3, 24A, 30, 32, 40: Brugel, Böhm, & Mannery (1981).
7, 11: Böhm & Solf (1990), only dereddened fluxes are listed [$E(B-V) = 0.40$]. [S II] 3726/29 fluxes from Böhm, Brugel, & Olmsted (1983).
34(ap.), HH34(MD), HH34(jet): Morse et al. (1993).
43A, 43B, 43C: Böhm & Solf (1990), only dereddened fluxes are listed [$E(B-V) = 0.20$, θ-Orionis extinction curve].
47A, 47C, 47D: Dopita, Schwartz, & Evans (1982).
49, 50, 54B, 54D, 56, 57: Schwartz & Dopita (1980).
83, 126B, 128: Ogura & Walsh (1991).
111V, 111L, 111D-J: Morse et al. (1993), Noriega-Crespo, Garnavich, & Raga (1993).
10, 184, 234, 235, 240: Goodrich (1986).
123: Reipurth & Heathcote (1990).
124, 125: Walsh, Ogura, & Reipurth (1992).
154, 158: Cohen & Fuller (1985).

TABLE 2

$E(B-V)$ FOR REDDENING CORRECTIONS

HH	$E(B-V)$	Method[a]	Reference[b]	HH	$E(B-V)$	Method[a]	Reference[b]
1	0.43	1	SBR88	49	0.38	2,3	SD80
2A	0.37	1	BBM81	50	0.69	2,3	"
2G	0.44	1	"	54B	0.78	2,3	"
2H	0.34	1	"	54C	1.03	2,3	"
3	0.45	1	"	56	0.59	2,3	"
7	0.40	2	BS90	57	0.84	2,3	"
11	0.40	2	"	83B,D	0.48	2	OW91
24A	0.71	1	BBM81	111V	0.70	2	M93
32	0.69	1	"	111L	0.90	2	"
34(ap)	0.41	2	M93	111D-J	0.90	2	"
34(MD)	0.41	2	"	123	0.41	3	RH90
34(jet)	0.41	2	"	124A-C	0.57	2	WOR92
40	0.70	1	BBM81	124D	0.15	2	"
43A[c]	0.20	4	SDC85	124E-F	0.02	2	"
43B[c]	0.20	4	"	125F	0.33	2	"
43C[c]	0.20	4	"	125I-K	0.52	2	"
47A	0.07	2	DSE82	126B	0.27	2	OW91
47C	0.48	2	"	128	0.82	2	"
47D	0.14	2	"	...	...	...	...

[a] Methods: (1) Miller's (1968); (2): from Hα/Hβ ratio; (3): from red and blue [O II] and/or [S II] ratios (Dopita, Binette, & Schwartz 1982); (4): from model fits to the optical continuum (Schwartz, Dopita, & Cohen 1985).

[b] References: SBR88 (Solf, Böhm, & Raga 1988); BBM81 (Brugel, Böhm, & Mannery 1981); BS90 (Böhm & Solf 1990); M93 (Morse et al. 1993); SDC85 (Schwartz, Dopita, & Cohen 1985); DSE82 (Dopita, Schwartz, & Evans 1982); SD80 (Schwartz & Dopita 1980); OW91 (Ogura & Walsh 1991); RH90 (Reipurth & Heathcote 1990); WOR92 (Walsh, Ogura, & Reipurth 1992).

[c] θ Orionis extinction curve was used.

responding to the measured values, and the second set corresponding to the dereddened values as given in the corresponding reference. A few of the spectra found in the literature have not been corrected for reddening (HH 10, 30, 154, 158, 184, 234, 235, and 240) and for these objects we only give the observed (not dereddened) spectrum. Finally, in a few cases only the dereddened spectra are given (HH 7, 11, 43A, 43B, and 43C), so that in our table we have only listed the dereddened line fluxes (these objects are indicated with an asterisk in Table 1).

In Table 2, we list the $E(B-V)$ values used for the reddening corrections of the different spectra. Also listed are the methods by which the $E(B-V)$ values have been derived, and the references of the relevant papers. From this table, it is clear that the reddening corrections are in many cases quite uncertain. For a few objects, the method of Miller (1968, in which the common upper level IR and blue [S II] lines are used) has been applied. Though this method in principle is expected to give the correct $E(B-V)$ values, in practice it gives somewhat uncertain results, due to the difficulty of obtaining reliable fluxes for the relevant lines. For other objects, ratios of red and blue [O II] and/or [S II] ratios have been used (Dopita, Binette, & Schwartz 1982), giving somewhat uncertain $E(B-V)$ determinations due to the fact that the line ratios are model dependent. In one case (HH 43), a comparison of the observed continuum spectrum with model predictions has been used to determine the $E(B-V)$. Finally, in most cases the value of $E(B-V)$ has been determined by assuming that the intrinsic Hα/Hβ ratio corresponds to the recombination cascade value. This is of course also quite uncertain, as it is expected that this line ratio will deviate appreciably from the recombination value for low velocity shocks (see, e.g., Hartigan et al. 1987).

Given these large uncertainties in the reddening corrections, we have chosen to concentrate on line ratios which are not strongly affected by reddening.

This can be easily done by considering the line ratios of the blue spectrum lines (see Table 1) to Hβ, and the ratios of the red spectrum lines to Hα. We see that for most objects, these line ratios have quite similar values whether the fluxes with or without reddening corrections are used. The most serious deviation is found for the [O II] (3726+3729)/Hβ ratio, which is quite strongly infuenced by reddening.

For example, for HH 54C (the most highly reddened object, see Table 2) the [O II] (3726 + 3729)/Hβ ratio increases by a factor of ~ 2.5 when the reddening correction is applied. It is clear that for the other line ratios of this particular object (and also for the ones of all of the other listed objects), the effect of the reddening correction is considerably smaller.

In this way, we have chosen a set of line ratios which are moderately reddening-independent, so that the errors in the reddening corrections should not be important. For the objects in which reddening corrections have been applied, we have calculated these line ratios with the dereddened fluxes. For the spectra which have not been corrected for reddening (in the relevant papers), we have calculated the line ratios with the measured fluxes, without attempting to carry out a correction for reddening. For these objects, we would expect to have errors of factors ~ 2 for the [O II] (3726+28)/Hβ ratio, and smaller errors for the other line ratios (see above).

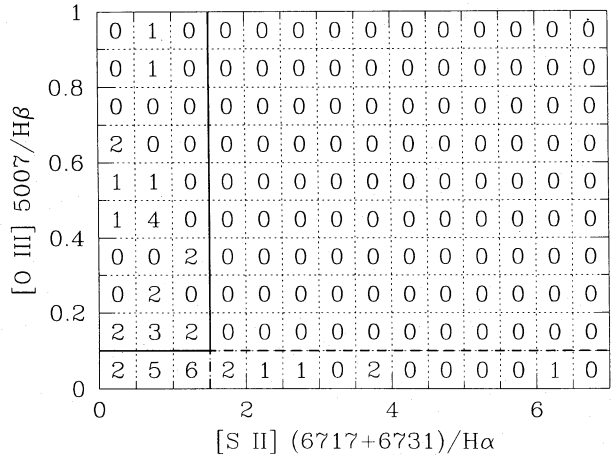

Fig. 1. Graph showing the [O III] 5007/Hβ versus [S II] (6717+6731)/Hα plane divided into boxes with $\Delta x = 0.5$ and $\Delta y = 0.1$. The number of HH spectra falling into the line ratio ranges limited by each box is drawn inside the corresponding box. All except 2 of the tabulated spectra (see Table 1) are included in this graph (see the text). It is clear that the objects fall into two main regions of the graph, one along the x-axis, and one along the y-axis (these two regions are enclosed by a thick dashed line and by a solid line, respectively). These two regions correspond to the low and high excitation spectra (respectively), and their intersection (in the region close to the origin) corresponds to the low excitation spectra.

3. CLASSIFICATION OF THE SPECTRA BASED ON THE [O III] 5007/Hβ AND [S II] (6717+6731)/Hα LINE RATIOS

In the literature, HH spectra have been losely classified according to their [O III] 5007/Hβ and [S II] (6717+6731)/Hα line ratios as "high excitation" (with strong [O III] 5007 and weak [S II] (6717+6731)), "intermediate excitation" (weak or absent [O III] 5007, relatively weak [S II] (6717+6731)) or "low excitation" (absent [O III] 5007, strong [S II] (6717+6731)). With the data set presented in the previous section, it is possible to derive quantitative limits on the [O III] 5007/Hβ and [S II] (6717+6731)/Hα ratios for these three spectroscopic categories.

Figure 1 shows the [O III] 5007/Hβ versus [S II] (6717+6731)/Hα plane, divided into rectangular boxes of sizes $\Delta y = 0.1$ and $\Delta x = 0.5$ (where y and x indicate the corresponding line ratios). Inside each of the boxes we have placed a number that indicates the number of spectra from our sample which have line ratios within the limits of the box.

From this graph it is clear that HH objects occupy two major regions, one region along the x-axis, and the other one roughly along the y-axis. From this result, a division into the three spectroscopic categories of HH spectra can be carried out as follows:

i) "high excitation" spectra, with [O III] 5007/Hβ > 0.1 and [S II] (6717+6731)/Hα ≤ 1.5,
ii) "intermediate excitation spectra", with [O III] 5007/Hβ ≤ 0.1 and [S II] (6717+6731)/Hα ≤ 1.5,
iii) "low excitation spectra", with [O III] 5007/Hβ ≤ 0.1 and [S II] (6717+6731)/Hα > 1.5.
Using these criteria, we would conclude that Figure 1 includes 22 high excitation, 13 intermediate excitation and 7 low excitation objects.

Three of the spectra listed in Table 1 are not included in Figure 1. HH 2A and G are not included because the flux of the [S II] 6731 line has not been measured. However, from their high [O III] 5007/Hβ and low [S II] 6717/Hα ratios we can safely classify them as "high excitation", giving us a total number of 24 high excitation spectra.

The remaining missing object is HH 47D, which has [O III] 5007/Hβ = 1.9 (the highest value for all of the spectra) and [S II] (6717+6731)/Hα = 2.0. As we will see in sections 4 and 5, all of the line fluxes other than the one of [O III] 5007 are consistent with a classification of HH 47D as a low excitation object. From this, we would conclude that the [O III] 5007 line flux might possibly be influenced by the surrounding H II region, as suggested by Dopita et al. (1982). We should also note that Hartigan,

Raymond, & Meaburn (1990) claim that the whole spectrum of HH 47D is quite uncertain, as all of the line intensities are very low. If we then go ahead and classify HH 47D as "low excitation", this would give us a total number of 8 low excitation objects.

From this, we conclude that of our sample of 45 spectra, 53% are "high excitation", 29% are "intermediate excitation" and 18% are "low excitation" spectra. In the following section, we will see that the objects divided into these three separate categories according to their [O III] 5007/Hβ and [S II] (6717+6731)/Hα ratios also form clearly separate groups when one analyzes other line ratios. There is of course a strong selection effect in our sample since on the average high excitation objects are brighter than low excitation objects, and are therefore more easily discovered.

4. A GENERAL ANALYSIS OF THE LINE RATIOS

Let us now consider a number of different line ratios that can be obtained from the spectra listed in Table 1. We have chosen:

i) five low excitation line ratios: [N I] (5198 + 5200)/Hβ, [O I] 6300/Hα, [S II] (6717+6731)/Hα, [Ca II] 7291/Hα, and [S II] (4068+4076)/Hβ, *ii)* four intermediate and high excitation line ratios: [O III] 5007/Hβ, [O II] (3726+3729)/Hβ, [Ne III] 3868/Hβ and [N II] 6583/Hα. As described in § 2, these line ratios have been taken either with respect to Hβ or Hα in such a way as to minimize the effect of errors in the reddening corrections.

In order to simplify the interpretation of the line ratios, we present them in eight line ratio scatter

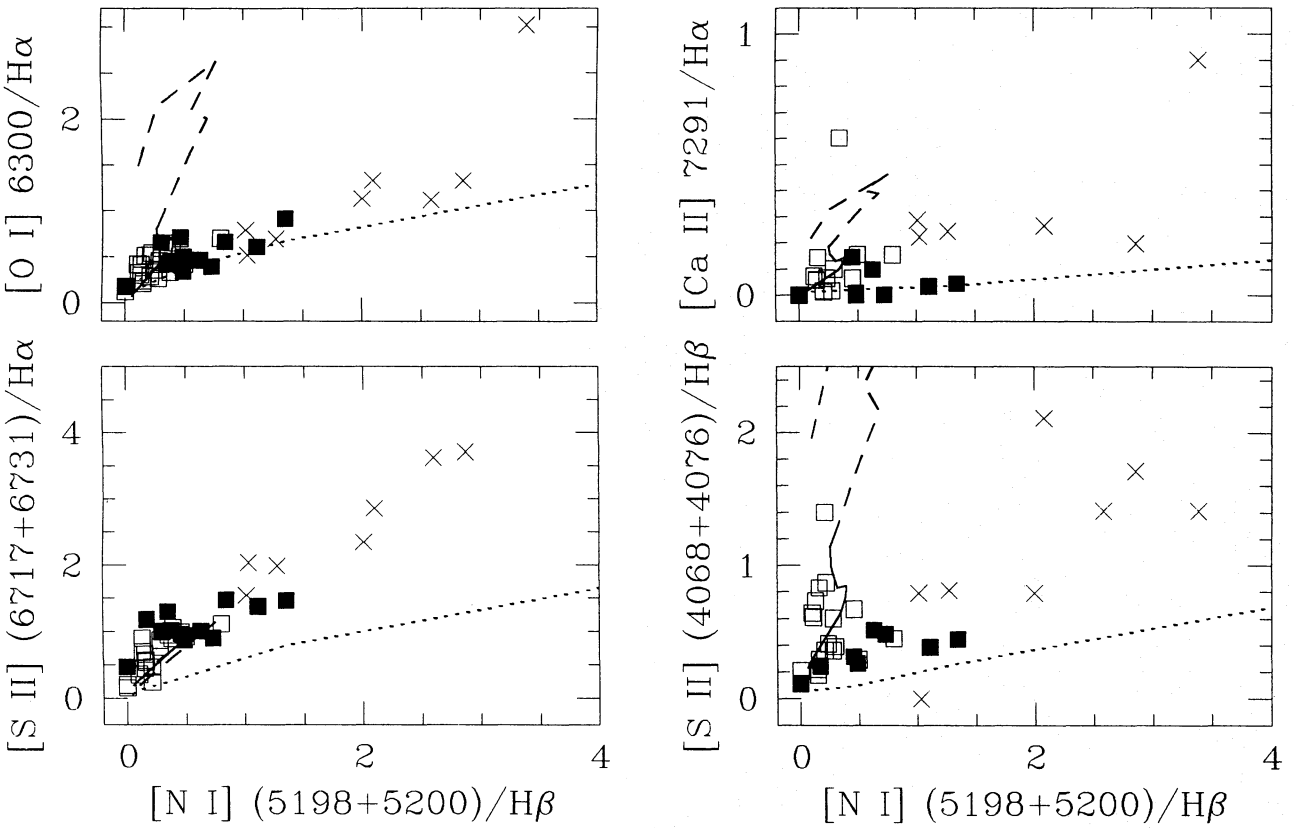

Fig. 2. Graph showing four scatter plots of low excitation line ratios as a function of [N I] (5198+5200)/Hβ. The points corresponding to the high excitation spectra are shown with open squares, the intermediate excitation spectra with solid squares, and the low excitation objects with crosses. Also plotted is a line connecting the points that are predicted from the sequence of "self consistent preionization", plane shock models of Hartigan et al. (1987). The models of shock velocities v_s = 20–100 km s^{-1} are connected with a dotted line, the ones of v_s = 100–200 km s^{-1} with a solid line, and the models of v_s = 200–400 km s^{-1} are connected with a dashed line.

plots (Figures 2 and 3) in which we always use [N I] (5198+5200)/Hβ as the abscissa, and the other chosen line ratios (a different one for each of the eight plots) as the ordinate. We have chosen the [N I] (5198+5200)/Hβ ratio as the abscissa because the [N I] (5198+200) line is one of the few that have been observed in most of the objects from our sample (in all of them except HH 126B, see Table 1). The other obvious possibility is to use the [S II] (6717+6731)/Hα ratio as the abscissa, but we have not done this because it confuses the comparisons that we will carry out with shock wave models.

Figure 2 shows scatter plots of four low excitation line ratios versus [N I] (5198+5200)/Hβ, and Figure 3 shows scatter plots of four high excitation ratios versus [N I] (5198+5200)/Hβ. In the same plots, we show a curve which joins the points predicted from the "self-consistent preionization" plane-parallel shock wave models of Hartigan et al. (1987). The models that we have chosen all have the same pre-shock density (n_{pre} = 100 cm^{-3}) and shock velocities ranging from 20 to 400 km s^{-1}. An idea of the shock velocities along the model curves can be obtained by noting that the [N I] (5198+5200)/Hβ ratio has the highest value for the v_s = 20 km s^{-1}shock model, and decreases monotonically with increasing shock velocity until v_s = 80 km s^{-1}, then slowly increases again (though not monotonically) until v_s = 300 km s^{-1}, and finally drops for higher shock velocities.

We see that the high, intermediate and low excitation objects form reasonably well defined groups in the line ratio scatter plots (Figures 2 and 3), except possibly for the [O II] (3726+3729)/Hβ and [N II] 6583/Hα versus [N I] (5198+5200)/Hβ graphs, in which the high and intermediate excitation spectra have basically undistinguishable line ratios. This result appears to strengthen the justification for the definition of three separate categories for HH spectra. It is also clear that while some of the line ra-

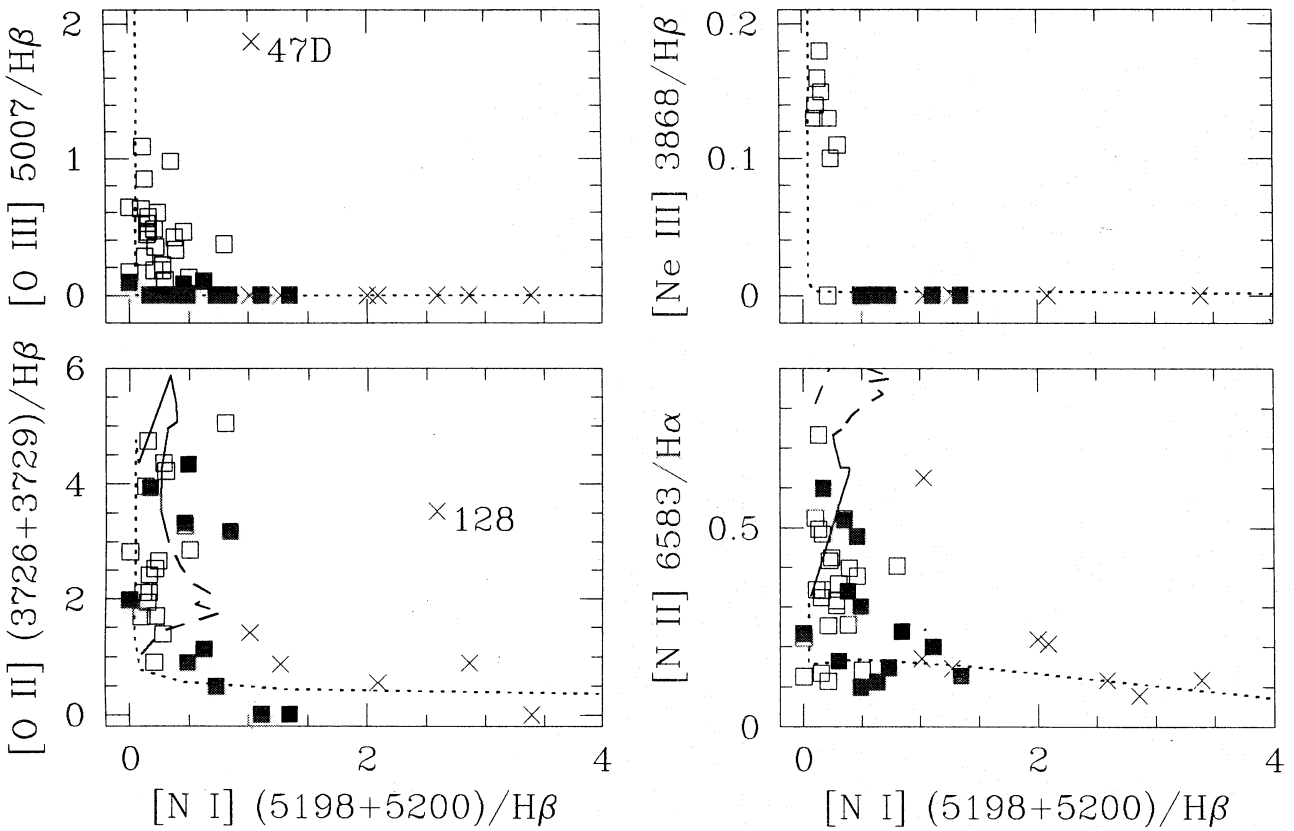

Fig. 3. Graph showing four scatter plots of intermediate and high excitation line ratios as a function of [N I] (5198+5200)/Hβ. The points corresponding to the high excitation spectra are shown with open squares, the intermediate excitation spectra with solid squares, and the low excitation objects with crosses. Also plotted is a line connecting the points that are predicted from the sequence of "self consistent preionization", plane shock models of Hartigan et al. (1987). The models of shock velocities v_s = 20–100 km s^{-1} are connected with a dotted line, the ones of v_s = 100–200 km s^{-1} with a solid line, and the models of v_s = 200–400 km s^{-1} are connected with a dashed line.

tios appear to be easily reproduced by shock models, others have clear problems. Interestingly, both the [O I] 6300/Hα versus [N I] (5198+5200)/Hβ scatter plot (see Figure 2) and the graphs of the intermediate and high excitation line ratios ([N II] 6583/Hα, [O II] (3726+3729)/Hβ, [O III] 5007/Hβ and [Ne III] 3868/Hβ) versus [N I] (5198+5200)/Hβ (see Figure 3) appear to be reasonably well reproduced by the shock wave models. On the other hand, in the scatter plots of [S II] (6717+6731)/Hα, [S II] (4068+4076)/Hβ and [Ca II] 7291/Hα versus [N I] (5198+5200)/Hβ substantial differences are found between the observed spectra and the model predictions (see Figure 2).

From this result, we would be tempted to conclude that there appears to be at least a partial problem with the model predictions of the [S II] (red and blue) and [Ca II] 7291 line fluxes. However, as we will discuss in section 6, more severe problems are found when trying to carry out a more detailed comparison between the observed and theoretical line ratios.

A particularly interesting result is obtained from the [S II] (6717+6731)/Hα versus [N I] (5198+5200)/Hβ scatter plot (Figure 2). The fact that low excitation objects have extremely high [S II] (6717+6731)/Hα values has been noted repeated times in the literature. The standard explanation for the difference between these values and the ones predicted, e.g., from the models of Hartigan et al. (1987) is that the models do not go to low enough shock velocities, for which higher [S II] (6717+6731)/Hα are expected. However, if we assume that at lower shock velocities a similar trend (in the [S II] (6717+6731)/Hα versus [N I] (5198+5200)/Hβ scatter plot) as the one of the 30 km s^{-1}and 20 km s^{-1}models is preserved, we would conclude that these lower shock velocity models would still not reproduce the observations (as we might have the correct [S II] (6717+6731)/Hα values, but the [N I] (5198+5200)/Hβ values would be too high by a large factor, see Figure 2).

Interestingly, we find that if we consider either the higher density plane shock models or the bow-shock models of Hartigan et al. (1987), this discrepancy between the model predictions and the observations does not disappear. It appears that predictions from shock models consistently have a [S II] (6717+6731)/Hα ratio too low by a factor of 2 or 3 with respect to the values observed in low and intermediate excitation HH objects (see Figure 2). We do not see a clear explanation for this effect.

Finally, we would like to point out that the scatter plots involving the low excitation lines show quite striking correlations (particularly for [S II] (6717+6731)/Hα and [O I] 6300/Hα versus [N I] (5198+5200)/Hβ, see Figure 2). This appears to imply that these line ratios depend mostly on one parameter, which probably is the shock velocity. One would have to conclude that all of the observed HH objects have preshock media of relatively similar densities (see also § 5). Also, one has to conclude that the geometry of the shock structure of the observed condensations is either similar for all objects (which seems to be not very reasonable) or unimportant for the formation of the lines (also somewhat unexpected).

The following section describes an analysis of other line ratios, which can be used directly as plasma diagnostics. We find that the results from this analysis again appears to agree (at least partially) with a family of models with different shock velocities (but otherwise identical parameters).

5. DIAGNOSTIC LINE RATIOS OF n_e

It is standard practice to use pairs of lines of the same ion to determine the electron density n_e and temperature T_e of the emitting region. Such determinations have been done for the spectra of some HH objects using a considerable number of line ratios (see, e.g., Brugel, Böhm, & Mannery 1981; Solf, Böhm, & Raga 1988). Unfortunately, many of these (mostly faint) diagnostic lines have not been observed in most of the published spectra.

The main diagnostic line ratio involving strong lines of a common ion is of course the red [S II] ratio. We have therefore used the n_e-sensitive [S II] 6731/6717 line ratio to determine electron densities for the objects of our sample (Table 1). In order to do this, we have assumed that the [S II] emitting region has a temperature $T_e = 10^4$ K, though of course our results are only weakly sensitive to T_e.

Figure 4 shows the electron densities for all of the spectra listed in Table 1, except for the ones of HH 2A and G (for which the [S II] 6731 flux has not been measured), plotted against the [N I] (5198+5200)/Hβ line ratio. In this graph we see a clear correlation of increasing n_e with increasing excitation (i.e., with decreasing values of [N I] (5198+5200)/Hβ). This effect is also seen in a family of shock models of the same preshock density (n = 100 cm^{-3}) and shock velocities v_s = 20–400 km s^{-1}(taken from Hartigan et al. 1987).

However, there is the following interesting discrepancy between the predicted and observed [S II] 6731/6717 line ratios. The HH objects that have [S II] 6731/6717 most closely approaching the low density limit are a few intermediate and high excitation objects (Figure 4), an effect which is not seen in the model spectra. We would therefore conclude that for these objects the preshock density probably has unusually low values. It is also surprising how small is the n_e variation for all intermediate and low excitation objects. From this we would conclude that the preshock densities cannot vary much from object to object.

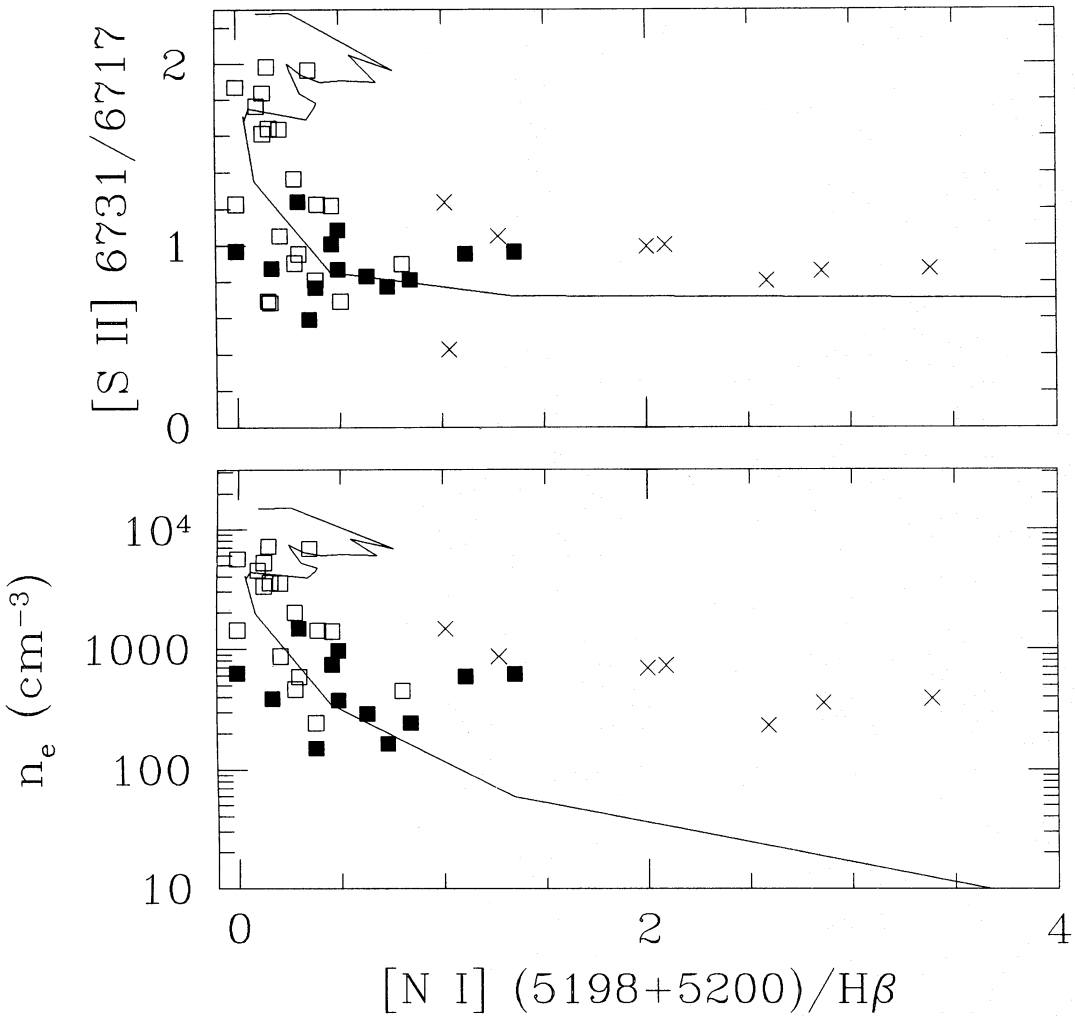

Fig. 4. Graph showing the [S II] (6717+6731)/Hα versus [N I] (5198+5200)/Hβ scatter plot (top) for the tabulated spectra (see Table 1) and the corresponding electron densities (bottom plot) deduced assuming a temperature of 10^4 K for the emitting gas. The points corresponding to the high excitation spectra are shown with open squares, the intermediate excitation spectra with solid squares, and the low excitation objects with crosses. Also plotted is a solid line connecting the points that are predicted from the sequence of "self consistent preionization", plane shock models of Hartigan et al. (1987).

6. A MORE DETAILED COMPARISON WITH SHOCK MODELS

Let us now discuss the results obtained from simultaneously analyzing several different line ratios (of different excitations) for each object of our sample. We have done this by choosing a shock model for fitting each of the points in the scatter plots discussed in § 4 (Figures 2 and 3), and then studying which are the required models for the different objects.

We have taken the the curves in the scatter plots predicted from the $n = 100$ cm^{-3} preshock density, self consistent preionization plane shock models of Hartigan et al. (1987, which cover a velocity range from 20 to 400 km s^{-1}), and found the shock velocity that best explains each of the observational points in the scatter plots (carrying out a simple, linear interpolation between the computed models when necessary). The results from this fitting procedure are shown in Figures 5 and 6.

The abscissas of these plots show the shock velocities that best fit the scatter plots involving the [O II] (3726+3729)/Hβ, [Ne III] 3868/Hβ, [S II] (4068+4076)/Hβ, [O III] 5007/Hβ, [O I] 6300/Hα, [N II] 6583/Hα, [S II] (6717+6731)/Hα and the [Ca II] 7291/Hα line ratios (also see Figures 2 and 3),

plotted with different symbols for the different line ratios. The results obtained for each object are offset from each other along the ordinate, and the identification of the corresponding object is given along the y-axis. We have divided the results into three plots, one containing the high excitation objects (Figure 5), a second one the intermediate excitation and a third one the low excitaion objects (both in Figure 6).

The high excitation objects (Figure 5) show very interesting effects. It is clear that for almost all of the objects, most of the emission line ratios are reproduced best by shock models with velocities very close to 100 km s^{-1}. The clear exception is the [S II] (6717+6731)/Hα ratio, which is best reproduced with considerably higher shock velocity models (in the 100–400 km s^{-1} range, see Figure 5). This clear discrepancy of the results obtained using the [S II] (6717+6731)/Hα ratio is not very surprising, given the fact that the shock models appear to have problems in reproducing this particular line ratio (see the discussion in § 4).

We should point out that there is a partial ambiguity in the [S II] (6717+6731)/Hα shock velocity determinations. It is clear from the [S II] (6717+6731)/Hα versus [N I] (5198+5200)/Hβ scatter plot of Figure 2 that the models with v_s = 100–200 km s^{-1} have line ratios very similar to the ones of the v_s = 200–400 km s^{-1} models. Because of this similarity of the predicted line ratios, the observed [S II] (6717+6731)/Hα line ratios would be repro-

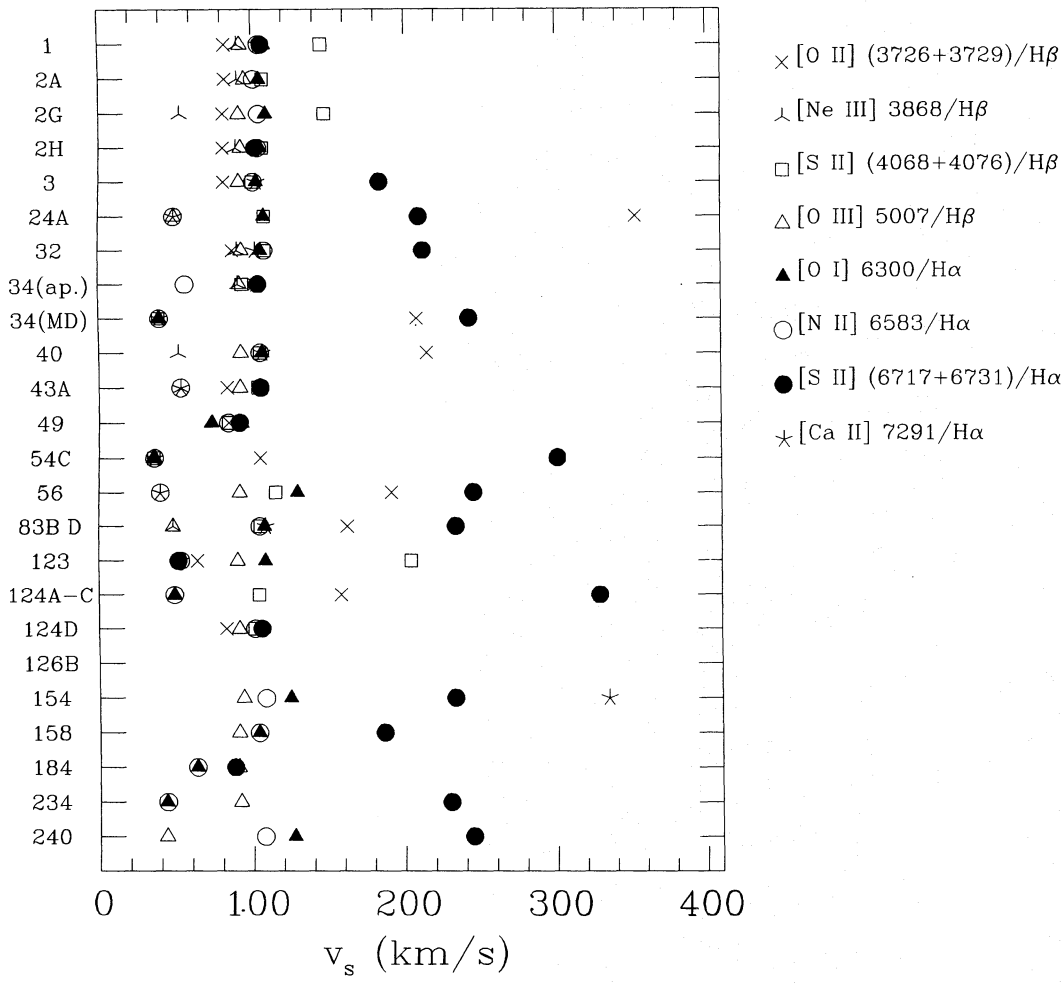

Fig. 5. Graph showing the shock velocities of the plane shock models that best fit the points in the line ratio scatter plots of Figures 2 and 3. This graph shows the results found for the high excitation spectra of our sample. The identification of the object is given along the ordinate, and the shock velocities needed to reproduce the different line ratios of the corresponding object are plotted along the abscissa (with different symbols for the different line ratios, as listed on the right of the plot).

duced with v_s = 100–200 km s^{-1} models almost as well as with v_s = 200–400 km s^{-1} models. A fit with the lower velocity models would at least partially remove the discrepancy between the shock velocity deduced from the [S II] (6717+6731)/Hα ratio, and the shock velocities deduced from the other line ratios (see Figure 5).

We are therefore tempted to exclude the [S II] (6717+6731)/Hα ratio, and to compute the average velocity obtained from the remaining line ratios. Carrying out an unweighted average over the shock velocities predicted for all objects (from all of the line ratios considered), we obtain an average velocity $\langle v_s \rangle$ = (82±37) km s^{-1}(where the error has been computed as the dispersion of all of the shock velocity determinations). In calculating this average, we have also not included the [O II] (3726+3729)/Hβ shock velocity determinations, as they also appear to behave peculiarly (see Figure 5). This may have been a consequence of the diffuse [O II] emission present, e.g., in the Orion region.

The small standard deviation of the shock velocity is a surprise (why do not larger shock velocities occur?). Our present sample confirms the conclusions drawn from a much smaller sample (Böhm 1995) that the [O III] 5007/Hβ (and also [Ne III] 3868/Hβ) line ratio in the high excitation objects never seems to indicate a shock velocity larger than 100 km s^{-1}. This surprising result is clearly visible in Figure 5.

For the low excitation objects (see Figure 6), a very good agreement is found between the shock velocities necessary for reproducing all of the line ratios in each object. In other words, the analyzed spectrum is fitted well by a single, plane shock model.

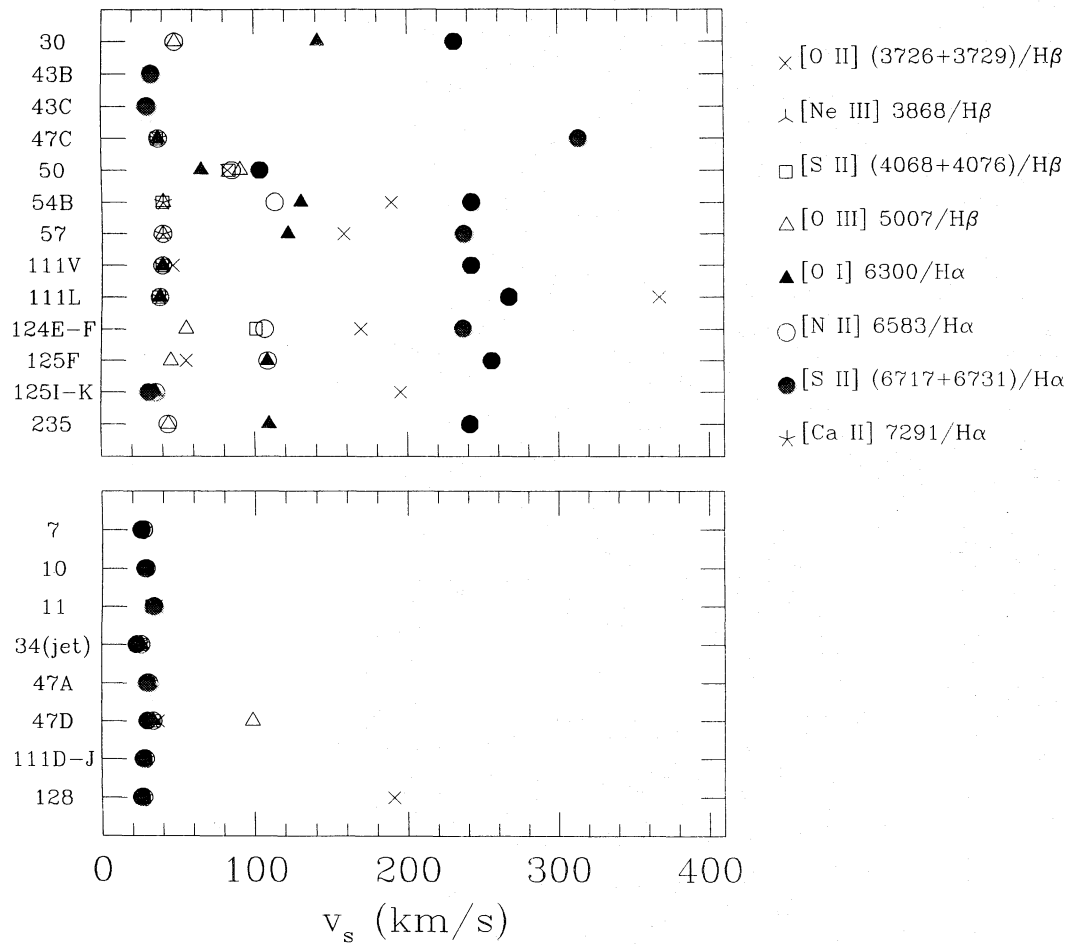

Fig. 6. Graph showing the shock velocities of the plane shock models that best fit the points in the line ratio scatter plots of Figures 2 and 3. This graph shows the results found for the intermediate excitation (top) and low excitation (bottom) spectra of our sample. The identification of the object is given along the ordinate, and the shock velocities needed to reproduce the different line ratios of the corresponding object are plotted along the abscissa (with different symbols for the different line ratios, as listed on the right of the plot).

If we compute the average shock velocity (averaged over all objects and line ratios, except the [S II] (6717+6731)/Hα and [O II] (3726+3729)/Hβ ratios), we obtain $\langle v_s \rangle = (31 \pm 10)$ km s^{-1}, quite surprisingly indicating that all of the low excitation objects have most similar shock velocities. The only drastic exception is the [C I] emission in HH 7, which differs from the theoretical predictions by a factor of ~ 10 (Böhm 1995).

The situation is somewhat more confused for the intermediate excitation objects (see Figure 6), in which the velocities predicted from some of the line ratios lie close to $v_s = 100$ km s^{-1}(similar to the high excitation objects) and others lie close to $v_s = 30$ km s^{-1}(similar to the velocity required for the low excitation models, see above). Here we again find that the shock velocities required by the [S II] (6717+6731)/Hα line ratios are substantially higher (~ 250 km s^{-1}, see Figure 6). If we compute an average shock velocity (as described above), we obtain a value $\langle v_s \rangle = (52 \pm 29)$ km s^{-1}, intermediate between the average shock velocities deduced for the high and the low excitation objects.

7. DISCUSSION

We have carried out a compilation of spectrophotometry of HH objects obtained by different authors over the past few decades. We present the compiled information in a table containing a number of lines ranging from the near UV to the near IR (see Table 1). The lines have been selected either because they are listed in a large part of the published spectra, or because they are of particular interest (e.g., because of a particularly high or low excitation). We have also listed [Fe II] and [Fe III] lines, that though not used in the present paper, are of special interest for the problem of iron abundance in HH objects (Beck-Winchatz, Böhm, & Noriega-Crespo 1994, 1996).

We suggest a division of the spectra into high excitation ([S II] (6717+6731)/H$\alpha \leq 1.5$; [O III] 5007/H$\beta > 0.1$), intermediate excitation ([S II] (6717+6731)/H$\alpha \leq 1.5$; [O III] 5007/H$\beta \leq 0.1$) and low excitation ([S II] (6717+6731)/H$\alpha > 1.5$), based on quantitative limits for the [S II] (6717+6731)/Hα and [O III] 5007/Hβ line ratios. We find that the spectra divided into these categories tend to have more or less well defined, common ranges for most of the line ratios that we have studied, as seen in the line ratio scatter plots of Figures 2 and 3.

These line ratio scatter plots also show the loci obtained from a family of plane shocks of different shock velocities (but otherwise identical parameters, taken from Hartigan et al. 1987), which seem to agree quite well with the location of the observed points. The most notable exception is the [S II] (6717+6731)/Hα ratio, which seems to be underestimated by the models by a factor of $\sim$ 2–3 (see Figure 2 and the discussion of § 4).

Interestingly, this discrepancy between the predicted and observed [S II] (6717+6731)/Hα ratios seems to be a problem restricted to HH objects, since shock excited spectra in SN remnants appear to have [S II] (6717+6731)/Hα ratios in good agreement with the model predictions (see Cantó 1981; Sabbadin, Minello, & Bianchini 1977). The high [S II] (6717+6731)/Hα line ratios of HH objects appear to be better reproduced by "truncated" shock models (such as the one computed for HH 43 and HH 47 by Dopita et al. 1982), indicating that the discrepancy between the models and the observations might possibly be due to the fact that the flow is non-stationary. On the other hand, it appears that models with different shock geometries could not reproduce the high observed [S II] (6717+6731)/Hα values, at least within the context of "quasi-one dimensional" models in which the flow is modeled as a superposition of one dimensional, oblique shocks.

We have also studied a diagnostic ratio giving estimates of n_e (§ 5). The values obtained for n_e show a somewhat similar trend (when plotted versus [N I] (5198+5200)/Hβ) to the predictions from the shock models (Figure 4). From this we would conclude that most HH objects appear to have similar preshock densities.

Finally, we have carried out plane shock model fits to all of the points in the scatter plots of Figures 2 and 3. Each of the fits gives an estimate of the shock velocity (as we have considered models with identical values for the other parameters), and the values obtained from all line ratios for all objects are shown in Figures 5 and 6.

We find that the results from these model fits are quite puzzling. A clear problem with our procedure is that we are comparing observations of emitting condensations with curved (and possibly time-dependent) shocks with plane, steady shock models. However, it seems that the effect of the curvature is probably not enough to explain the observed discrepancies between the observed and predicted line ratios. In a curved shock, the lower excitation lines have a stronger contribution from the more oblique, lower shock velocity regions, and the higher excitation lines are produced in the more perpendicular, higher shock velocity regions. We therefore expect the shock velocities required to reproduce the [O III] 5007/Hβ ratio with plane shock models to be higher than the shock velocities necessary to reproduce the [O I] 6300/Hα line ratio. Our sample of high excitation objects clearly shows the opposite effect, with a velocity $v_s \approx 90$ km s^{-1} required for reproducing [O III] 5007/Hβ and a velocity $v_s \approx 110$ km s^{-1} required for reproducing [O I] 6300/Hα. Considerably higher shock velocities are necessary for explaining the somewhat problematic [S II] (6717+6731)/Hα

line ratio (see Figure 6), though this might be a result of the fact that the [S II] (6717+6731)/Hα values of models with $v_s = 100$–200 km s^{-1} are very similar to the ones of models with $v_s = 100$–200 km s^{-1}.

An even stronger problem appears to be that the shock velocities predicted from the [O III] 5007/Hβ and [Ne III] 3868/Hβ line ratios cluster between 90 and 100 km s^{-1} for all of the high excitation objects. These line ratios never indicate a shock velocity larger than 100 km s^{-1} (see Figure 5). If taken at face value, these results would indicate that there is a mechanism by which a maximum shock velocity of $\sim$ 100 km s^{-1} is selected by all of the high excitation objects. Also quite surprising is the fact that the spectra of all low excitation objects are reproduced well by models with a very narrow (20–40 km s^{-1}) shock velocity range (see Figure 6).

This result is the most serious discrepancy that we find between our compiled spectrophotometric data set and the predictions from shock models. The observed spectra of HH objects fall into two categories (high and low excitation) of quantitatively very similar spectra. On the other hand, the shock wave models predict a range of different spectra (most strongly influenced by the value of the shock velocity), and by no means reproduce the apparent "bimodal" nature of high and low excitation HH spectra. We feel that it is more cautious at this time not to speculate on the possible explanations for this discrepancy.

Finally, we should note that serious problems are also found in the interpretation of the intermediate excitation spectra. For many of these spectra we find that a shock velocity of $\sim$ 100–140 km s^{-1} is required for explaining the [O I] 6300/Hα, while a velocity of only $\sim$ 30–60 km s^{-1} is implied by the [O III] 5007/Hβ ratio. It appears to be impossible to reproduce such results with a superposition of different plane shock models.

We would like to thank an anonymous referee for very helpful comments and suggestions. This work has been supported by the CONACyT grant 0177P-E9506.

REFERENCES

Beck-Winchatz, B., Böhm, K.H., & Noriega-Crespo, A. 1994, PASP, 106, 127
Beck-Winchatz, B., Böhm, K.H., & Noriega-Crespo, A. 1996, AJ, 111, 346
Böhm, K.H. 1995, in Shocks in Astrophysics, ed. T.J. Millar & A.C. Raga (Dordrecht: Kluwer), 11
Böhm. K.H., Brugel, E.W., & Olmsted, E. 1983, A&A, 125, 23
Böhm, K.H., & Solf, J. 1990, ApJ, 348, 297
Brugel, E.W., Böhm, K.H., & Mannery, E. 1981, ApJS, 47, 117
Cantó, J. 1981, in Investigating the Universe, ed. F. Kahn (Dordrecht: Reidel), 95
Cohen, M., & Fuller, G.A. 1985, ApJ, 296, 620
Dopita, M.A., Binette, L., & Schwartz, R.D. 1982, ApJ, 261, 183
Dopita, M.A., Schwartz, R.D., & Evans, I. 1982, ApJ, 263, L73
Edwards, S., Ray, T., & Mundt, R. 1993, in Protostars and Planets III, ed. E.H. Levy & J.I. Lunine (Tucson: The Univ. of Arizona Press)
Goodrich, R.W. 1986, AJ, 92, 885
Hartigan, P., Raymond, J.C., & Hartmann, L. 1987, ApJ, 316, 323
Hartigan, P., Raymond, J.C., & Meaburn, J. 1990, ApJ, 362, 624
Miller, J.S. 1968, ApJ, 154, L57
Morse, J.A., Heathcote, S., Hartigan, P., & Cecil, G. 1993, AJ, 106, 1139
Noriega-Crespo, A., Garnavich, P.M., & Raga, A.C. 1993, AJ, 106, 1133
Ogura, K., & Walsh, J.R. 1991, AJ, 101, 185
Raga, A.C. 1995, in Disks, Outflows and Star Formation, ed. S. Lizano & J.M. Torrelles, RevMexAASC, 1, 103
Ray, T.P., & Mundt, R. 1993, in Astrophysical Jets, ed. D. Burgarella, M. Livio, & C. O'Dea (Cambridge: Cambridge Univ. Press), 145
Reipurth, B. 1994, A General Catalogue of Herbig-Haro Objects, electronically published via anon.ftp to ftp.hq.eso.org, directory /pubs/Catalogs/Herbig-Haro
Reipurth, B., & Cernicharo, J. 1995, in Disks, Outflows and Star Formation, ed. S. Lizano & J.M. Torrelles, RevMexAASC, 1, 43
Reipurth, B., & Heathcote, S. 1990, A&A, 229, 527
_____. 1993, in Astrophysical Jets, ed. D. Burgarella, M. Livio, & C. O'Dea (Cambridge: Cambridge Univ. Press), 35
Sabbadin, F., Minello, S., & Bianchini, A. 1977, A&A, 60, 147
Schwartz, R.D. 1975, ApJ, 195, 631
Schwartz, R.D., & Dopita, M.A. 1980, ApJ, 236, 543
Schwartz, R.D., Dopita, M.A., & Cohen, M. 1985, AJ, 90, 1820
Solf, J., Böhm, K.-H., & Raga, A.C. 1988, ApJ, 334, 229
Walsh, J.R., Ogura, K., & Reipurth, B. 1992, MNRAS, 257, 110

Karl-Heinz Böhm: Department of Astronomy FM-20, University of Washington, Seattle, WA 98195 USA. (bohm@astro.washington.edu)
Jorge Cantó and Alejandro C. Raga: Instituto de Astronomía, UNAM, Apartado Postal 70-264, 04510 México, D.F., México. (raga@astroscu.unam.mx)